Article:
Elliott, JR, Jolivet, R, González, PJ et al. (4 more authors) (2016) Himalayan megathrust geometry and relation to topography revealed by the Gorkha earthquake. Nature Geoscience, 9 (2). pp. 174-180. ISSN 1752-0894

https://doi.org/10.1038/NGEO2623

Himalayan Megathrust Geometry and Relation to Topography Revealed by the Gorkha Earthquake

J. R. Elliott[1*], R. Jolivet[2], P. J. González[3], J.-P. Avouac[2,4], J. Hollingsworth[5], M. P. Searle[6], V. L. Stevens[4].

Large thrust faults accommodate crustal shortening caused by tectonic forces, contributing to the growth of topography over geological timescales. The Himalayan belt has been the locus of some of the largest earthquakes on the continents, including the recent 2015 magnitude 7.8 Gorkha earthquake. Competing hypotheses exist to explain how topography is sustained and how the current convergence across the Himalaya is accommodated — whether predominantly along a single thrust or from more distributed, out-of-sequence faulting. Here we use geodetically-derived surface displacements to show that whilst the Gorkha earthquake was blind, it ruptured the Main Himalayan Thrust (MHT), highlighting its ramp-and-flat geometry. Reconciling a wide variety of independent geological, geomorphological, geophysical and geodetic observations, we quantify the geometry of the MHT in the Kathmandu area. Present-day convergence across the Himalaya is mostly accommodated along the MHT, and no out-of-sequence thrusting is required to explain the higher uplift and incision rates at the front of the high range. In addition to the region west of the Gorkha rupture, a large portion of the MHT remains unbroken south of Kathmandu presenting a continuing seismic hazard. Constraining the geometry of the structure accommodating most of the convergence is a landmark for further studies on the development of the Himalayan range and on the seismic behaviour of the broader region of Nepal.

On the 25th April 2015, a Mw 7.8 earthquake struck Nepal, rupturing beneath the higher parts of the Himalayas and resulting in over 8,800 fatalities (Fig. 1). Initial seismological observations showed that the rupture initiated beneath the Gorkha region of Central Nepal at 15 km depth, consistent with a low-angle thrust fault dipping at ∼11° north. Finite fault rupture models from the USGS NEIC indicate that the rupture propagated eastward beneath Kathmandu for about 140 km. Early observations[1–4] suggest the rupture did not reach the surface, contrasting with earlier events, such as the 1934 and 1255 Mw 8+ earthquakes in the same area[5] or the 2005 Mw 7.6 Kashmir earthquake at the western end of the Himalaya[6]. A pair of Mw 6.6–6.7 aftershocks occurred within the hour following the mainshock, at either end of the rupture (Fig. 1). An even larger aftershock (Mw 7.3) occurred at the north-eastern end of the main rupture 17 days later, resulting in

further fatalities.

The 2015 Gorkha earthquake occurred within a gap in historical seismicity[7;8] (Fig. 1). The most recent major earthquake in Nepal was the 1934 Ms ~8.2 Nepal-Bihar earthquake, which initiated 175 km east of Kathmandu[9] and propagated westward for approximately 150 km, causing severe shaking in eastern Nepal and the Ganga plain[7]. Given its large magnitude, the location of its epicentre and the paleo-seismological evidence for surface breaks[5], the 1934 event likely ruptured the entire seismogenic thickness, from the aseismic shear zone to the surface. In the area of the Gorkha earthquake, a series of three large (M7+) earthquakes occurred in 1833[8], resulting in intense shaking around Kathmandu and to the south, but tapering off quickly to the north (Supplementary Fig. 1). While the spatial relationship between these different earthquakes is challenging, especially in the pre-instrumental period, it is clear that the 2015 earthquake only ruptured a small portion of the MHT, at the eastern edge of the 800 km wide seismic gap between the 1905 M 7.8 Kangra earthquake in the west and the M 8.2 1934 earthquake in the east[10] (Fig. 1b). Given that the last event to have ruptured such a long portion of the megathrust was the 1505 Mw 8.2 earthquake[7;11], affecting Western Nepal and North-West India, the intervening 500 years has resulted in the accumulation of a 10 m slip deficit[12].

The Gorkha earthquake provides an opportunity to investigate the role of seismic deformation in building the Himalaya: how the fault activated in this earthquake relates to the structure of the wedge and how the current topography of the range has developed. The Himalaya is an orogenic wedge formed by a stack of thrust sheets scraped off Indian crust as it was underthrust beneath the margin of Asia after closure of the Tethys ocean[13]. All thrust faults within the wedge sole into a main basal décollement which coincides with a mid-crustal reflector at a depth of about 40 km beneath southern Tibet[14;15]. Debate is ongoing regarding how the wedge is deforming and the reason for the steep front of the high range lying about 100 km north from the southern end of the wedge (Fig. 1). Some authors have argued that the location of the front of the high topography could be explained by a mid-crustal ramp along the MHT[16;17], or by a combination of ramp overthrusting and underplating associated with duplex development of the Himalayan wedge[18;19]. Conversely, others have argued for active out-of-sequence thrusting at the front of the high Himalaya[20;21].

We combine radar and optical satellite images to measure ground displacements and determine the geometry and kinematics of thrust faulting for the Himalayas. We process Interferometric Synthetic Aperture Radar (InSAR) data from the European Space Agency (ESA) Sentinel-1 satellite to derive surface line-of-sight ground motion (Fig. 2, Supplementary Fig. 2 and Table 1) and surface offsets (Supplementary Fig. 3) from the correlation of amplitude images from both SAR and Landsat-8 (see Methods). We supplement these observations with other published surface displacements from the ALOS-2 SAR satellite[3], and GPS coseismic

offsets[2] (Supplementary Fig. 4). We observe up to 2 m of south-south-west motion and almost 1 m of uplift in the Kathmandu basin and the surrounding Lesser Himalaya, whilst north of this, a large region of the Higher Himalaya subsided by about 0.6 m (Fig. 2).

The low gradient in the surface displacement field measured from both radar (Fig. 2 and Supplementary Fig. 2) and optical offset images (Supplementary Fig. 3) is consistent with slip during the 2015 Gorkha earthquake remaining buried at depth along the entire 150 km rupture length. None of the satellite geodetic measurements (i.e. from InSAR, SAR azimuth correlation and optical image correlation) show surface slip associated with the MFT. However, triggered near surface slip is imaged with the Sentinel-1 coseismic interferograms (Fig. 2d and Supplementary Fig. 5) along a 26 km long discontinuity, 10 km north of the MFT. This discontinuity in the interferometric phase follows the trace of the Main Dun Thrust (MDT), a relatively minor splay considered to be less active than the MFT[22]. Independent interferograms on two overlapping descending tracks with acquisitions made 4 and 11 days after the mainshock show broadly consistent surface offsets, peaking with 6 cm of surface uplift along the radar line-of-sight. This surface displacement field at the fault trace is consistent with 12 cm of reverse slip, assuming a 30° northward-dipping plane[22], and happened during or shortly (i.e. less than 4 days) after the mainshock. In the intervening 7 days before another SAR acquisition on a parallel track, fault slip along the central portion (5 km long) continued by a further ∼2.5 cm upward motion along the radar line-of-sight (Fig. 2e), highlighting postseismic slip on this secondary structure.

We seek to explore the range of possible geometries of the MHT explaining the surface displacement data of the mainshock (Fig. 3), accounting for what is currently known about the fault geometry at depth. From south to north, our fault model includes three segments to reflect the ramp-flat-ramp geometry: (1) a shallow 30° north dipping ramp between the surface and 5-km-depth, constrained by structural sections in the area and approximately following the surface trace of the MFT[22] with a strike of N108°, (2) a flat portion with a shallow angle reaching a (3) steeper, mid-crustal, ramp. We systematically test a range of possible values of dip angles of the flat (1–10°) and the mid-crustal ramp (1–45°) together with possible horizontal distances for the hinge-line defined by the top of the mid-crustal ramp and the MFT (50–120 km). For each case, we solve for the distribution of dip slip using a standard constrained least-squares approach and compute a weighted misfit for that solution (here the log-likelihood, see Methods and Supplementary Fig. 6). We consider that all geometric configurations giving a weighted misfit within 95% of the best configuration are acceptable models.

Within these bounds, the most likely dip angle for the flat portion of the MHT is constrained between 5 and 8° north. This geometry fits with the zone of high electrical conductivity imaged from magneto-telluric data[23] (Fig. 4), corresponding to wet sediments dragged along the MHT.

Further north, fault geometries consistent with surface geodetic data extend from (1) models with no significant change in the dip angle (i.e. no steep, mid-crustal, ramp) to (2) models with a steep, mid-crustal, ramp. Although the peak distribution in changes of dip angle between the flat and the ramp segments for acceptable models is around a 5–7° increase (Fig. 3), the geodetic data alone do not exclude the hypothesis of a flat MHT all the way into the Tibetan Plateau (Supplementary Fig. 7). However, additional data advocate for a steep, mid-crustal, structure north of the Kathmandu basin. From interseismic GPS- and leveling-derived rates of motion, we use a Bayesian approach to infer the PDF of the location of the dislocation explaining elastic strain increase during the interseismic period (see Fig. 3, Methods and Supplementary Fig. 8). The tip of this aseismic shear zone (20–25 km, consistent with the location of the main reflector in the InDepth seismic reflection profile[15]) cannot be shallower than 15 km, while coseismic slip concentrates between 5 and 15 km depth, highlighting a clear depth separation between coseismic slip (5–15 km), the micro-seismic activity (15–20 km) and the aseismic shear zone (20–25 km). The same argument can be made for a similar separation in the direction perpendicular to the MHT (Fig. 3). Such offset requires a steep, mid-crustal, ramp connecting the flat seismogenic portion of the MHT to the deep, aseismic, shear zone.

Then, considering the case of a 15–25° north-dipping mid-crustal ramp, the position of its shallow tip is constrained by surface coseismic displacements (80–90 km north of the MFT, Supplementary Fig. 6)). This position of the hinge line between ramp and flat also fits with the location of the high-frequency sources (Fig. 1 and Fig. 4) imaged by back-projection of teleseismic P waves[1]. This is consistent with a direct structural control on generating these seismic sources. By reconciling co- and inter-seismic geodetic surface displacements, micro-seismic activity and previous geological interpretations of structure and river incisions, we propose the following detailed fault geometry of the MHT from south-to-north under the Kathmandu area (Fig. 4):

1. a 30° north dipping ramp from the surface (outcropping as the MFT) to 5 km depth followed by
2. a 75-km-wide, 7°, north dipping flat section that ends on a
3. 20° north dipping, 30 km wide, mid-crustal ramp that intersects
4. a shallow north dipping shear zone of aseismic deformation, which coincides well with the deeper portion of the MHT imaged seismically[15;24].

The maintenance of the steep front of the high Himalayan range probably owes itself to the mid-crustal ramp along the MHT. This transition zone also coincides with the down-dip edge of the locked zone (Fig. 1) as determined by measurements of interseismic strain[12;25]. All together our proposed geometry of the MHT satisfies very well previous geophysical constraints, and is also consistent with geomorphic and geological

structural constraints for the Himalaya, allowing us to propose a unified cross-section across the range, from the Indian plain in the south to the Tibetan Plateau in the north (Fig. 5). Of particular note, the ramp position is consistent with field observations of broadly folded foliations north of the Kathmandu Klippe thought to be related to duplex development in the Lesser Himalaya, as proposed along a number of geological cross sections across Nepal[26]. Our proposed fault geometry matches remarkably well the geometry of the MHT inferred from thermo-kinematic models adjusted to thermo-barometric and thermo-chronological data[19;27] or to one inferred from river incision[16]. Coseismic slip is constrained to the MHT at depth, with no out-of-sequence thrusting on the MCT (Fig. 5). Within error, the present rate of interseismic shortening[25] matches the long-term slip rate on the MFT[22], excluding the possibility of substantial internal deformation of the wedge. Co- or early post-seismic near-surface slip on the MDT is the only detectable evidence of deformation off the MHT and corresponds to only ∼10 cm of horizontal shortening, almost two orders of magnitude smaller than the deformation due to slip on the MHT. This is consistent with southward propagation of the thrust front through time from the MCT (active between 20–15 Ma[28]), Ramgarh thrust (RT, active ∼15–10 Ma), to the Main Boundary thrust (MBT, active from ∼7–0 Ma), and eventually to the southernmost MFT[22] (Fig. 5).

The slip distribution calculated for the proposed geometry shows peak slip of about 8 m, for a 140 km-long, 50–60 km-wide rupture (Fig. 1 and Fig. 4), with more than 60% of the released moment located southward (i.e. up-dip) of the main cluster of pre-seismic micro-earthquakes and surrounded by aftershocks. Slip from the largest (Mw 7.3) aftershock that occurred 17 days later fills in most of the eastern gap in the slip contours at the lower down-dip edge of the fault rupture (Fig. 1 and Supplementary Fig. 12), where the aftershock activity was high early on. This major aftershock highlights a filling in of a gap in the mainshock slip in the east after some delay, potentially caused by a rupture impeding barrier of unknown origin (aseismic slip, geometrical complexity or low stress level).

Whilst most of the slip during the Gorkha earthquake occurred on the shallow flat portion of the MHT, slip tapers out on the mid-crustal ramp where interseismic creep is inferred to extend. This either suggests the ramp slips in a mixture of seismic and aseismic behaviour, or that there is a broad zone of deformation over a 20×10 km region. However, no out-of-sequence thrusting in the high range is seen during the Gorkha earthquake, nor is it needed to explain the locally higher uplift and incision rates at the front of the high range given the location we find for the mid-crustal ramp. The northern limit of slip is contained within the locked zone (Fig. 1), which is consistent with the generic, globally observed, behavior of active faults and megathrusts, in which seismic and aseismic portions appear mutually exclusive[29–31]. This would lead to a maximum possible rupture width of ∼100 km in this region[25]. At the shallow end of the rupture, slip tapers off over the relatively short distance of 5 km on the flat from greater than 3 m to less than 1 m at 11 km

depth, no closer than 50 km from the MFT (Fig. 1). This abrupt up-dip limit of slip is markedly uniform along strike for the 140 km length rupture, and at a near constant depth of 11 km, where the sensitivity of our slip model is high. What controls the arrest of the rupture is not clear since this portion of the fault is locked during the pre-seismic period[12;25], and hence is anticipated to fail during an earthquake. Such a sharp up-dip limit on slip could result from the soleing out of other thrusts such as the MBT onto the MHT (Fig. 5), resulting in branch lines forming a structural complexity on the MHT interface forming a wide damage zone impeding up-dip propagation for earthquake ruptures. This leaves a locked fault width that is at least as wide as that which ruptured in the 2015 earthquake (Fig. 4), but at a shallower depth. Similar constrained deeper slip leaving wide unruptured fault segments at shallower depths have been seen in smaller continental reverse earthquakes elsewhere[32] — in one case resulting in the continuation of seismic rupture after a one year delay[33], the hiatus in that case likely due to the interaction of the rupture plane with other intersecting fault segments at depth. Alternatively, a reduced stress level left from past earthquakes may also have limited the extent of the rupture. To the east, the 1934 Bihar-Nepal earthquake is thought to have ruptured the whole seismogenic depth, reaching the surface and reducing the stress level there. If this earthquake were to have propagated near the surface to the west (a possibility which cannot be excluded by[5]), it would have also left a stress shadow up-dip of the Gorkha earthquake rupture. More accurate constraints on the extent of historic ruptures is key in addressing the role of stress shadowing along the MHT.

The Himalaya rise over 5 km above the plains of India; their great height a result of crustal thickening due to the northward collision of India with Asia over millions of years. As a consequence of the Gorkha earthquake, however, the high range subsided by up to 60 cm (Supplementary Fig. 11), as a result of elastic extension north of the region of maximum southward slip as imaged in our model (Fig. 2c and Fig. 5). Since the rest of the locked portion of the MHT, prone to rupture in earthquakes, is located even further southward from the main slip zone found here, we can assume that all major thrusting seismic events in the region will tend to lower the high Himalayan topography. However, on average, over multiple earthquake cycles, the long term uplift of the High Himalaya is about 4 mm/yr[19].

The peak uplift rate in the High Himalaya relative to Gangetic plain measured from levelling[34] and InSAR[35] over recent decadal timescales is about 7 mm/yr, larger than the 4 mm/yr long term uplift for the High Himalaya[19]. The difference might be due to co-seismic subsidence observed during the Gorkha earthquake (up to 60 cm) and expected from future earthquakes (the locked portion of the MHT lies south of the high chain). We therefore conclude that long-term uplift of the high chain occurs primarily in the time period between large earthquakes on the MHT. Current geodetic shortening rates[12;25] agree with longer term slip rates on the MHT. Furthermore, assuming our preferred fault geometry is correct, the contribution

of elastic deformation to uplift predicted from the projection of the regional distribution of coupling on our geometry[25] matches with the uplift rates in the interseismic period[34] (Supplementary Fig. 9). Therefore, only a small fraction of the interseismic strain translates into permanent deformation. Consequently, the 3–4 mm/yr long-term uplift at the front high chain, must primarily result from ramp overthrusting during transient episodes of deformation. Post-seismic slip could be an efficient way of building topography at the front of the chain and the next few years of observations will allow to verify this hypothesis.

We have reconciled a suite of independent observations of Himalayan faulting and derived a proposed geometry of the MHT satisfying geological, geophysical and geomorphic constraints gathered from numerous studies. This understanding of the fault geometry may now be used as a basis for further investigation on the seismogenic behaviour of the Himalayan front in the region of Kathmandu, as well as a starting point for long-term models for building of the highest mountain range in the world. Our results also highlight the potential for structural control on the propagation and arrest of earthquake rupture fronts: i.e. in the generation of high frequency seismic waves along the hinge line defining the ramp-flat transition; and the possible arrest of up-dip rupture from branching faults soleing into the MHT. The latter finding highlights a large, shallow region of the MHT south of Kathmandu that has not ruptured in this event, but is locked, and therefore still has the potential to fail seismically.

Methods Methods and any associated references are available in the online version of the paper.

References

[1] Avouac, J.-P., Meng, L., Wei, S., Wang, W. & Ampuero, J.-P. Lower edge of locked Main Himalayan Thrust unzipped by the 2015 Gorkha earthquake. *Nature Geosciences* (2015).

[2] Galetzka, J. *et al.* Slip pulse and resonance of the Kathmandu basin during the 2015 Gorkha earthquake, Nepal. *Science* **349**, 1091–1095 (2015).

[3] Lindsey, E. *et al.* Line of Sight Displacement from ALOS-2 Interferometry: Mw 7.8 Gorkha Earthquake and Mw 7.3 Aftershock. *GRL* (2015).

[4] Wang, K. & Fialko, Y. Slip model of the 2015 Mw 7.8 Gorkha (Nepal) earthquake from inversions of ALOS-2 and GPS data. *GRL* (2015).

[5] Sapkota, S. N. *et al.* Primary surface ruptures of the great Himalayan earthquakes in 1934 and 1255. *Nature Geosciences* **6**, 71–76 (2013).

[6] Avouac, J.-P., Ayoub, F., Leprince, S., Konca, O. & Helmberger, D. V. The 2005, M_w 7.6 Kashmir earthquake: Sub-pixel correlation of ASTER images and seismic waveforms analysis. *EPSL* **249**, 514–528 (2006).

[7] Ambraseys, N. N. & Douglas, J. Magnitude calibration of north Indian earthquakes. *GJI* **159**, 165–206 (2004).

[8] Bilham, R. Earthquakes in India and the Himalaya: tectonics, geodesy and history. *Annals of Geophysics* **47**, 839–858 (2004).

[9] Chen, W.-P. & Molnar, P. Seismic moments of major earthquakes and the average rate of slip in central Asia. *JGR* **82**, 2945–2970 (1977).

[10] Bilham, R., Gaur, V. K. & Molnar, P. EARTHQUAKES: Himalayan Seismic Hazard. *Science* **293**, 1442–1444 (2001).

[11] Ambraseys, N. & Jackson, D. A note on early earthquakes in northern India and southern Tibet. *Current Science* **84**, 570–582 (2003).

[12] Ader, T. *et al.* Convergence rate across the Nepal Himalaya and interseismic coupling on the Main Himalayan Thrust: Implications for seismic hazard. *JGR* **117**, B04403 (2012).

[13] Searle, M. P. *et al.* The closing of Tethys and the tectonics of the Himalaya. *GSAB* **98**, 678–701 (1987).

[14] Hauck, M. L., Nelson, K. D., Brown, L. D., Zhao, W. & Ross, A. R. Crustal structure of the Himalayan orogen at 90 east longitude from Project INDEPTH deep reflection profiles. *Tectonics* **17**, 481–500 (1998).

[15] Nábělek, J. *et al.* Underplating in the Himalaya-Tibet collision zone revealed by the Hi-CLIMB experiment. *Science* **325**, 1371–1374 (2009).

[16] Lavé, J. & Avouac, J. P. Fluvial incision and tectonic uplift across the Himalayas of central Nepal. *JGR* **106**, 26561–26591 (2001).

[17] Pandey, M. R., Tandukar, R. P., Avouac, J. P., Lave, J. & Massot, J. P. Interseismic strain accumulation on the Himalayan Crustal Ramp (Nepal). *GRL* **22**, 751–754 (1995).

[18] Bollinger, L. *et al.* Thermal structure and exhumation history of the Lesser Himalaya in central Nepal. *Tectonics* **23**, TC5015 (2004).

[19] Herman, F. *et al.* Exhumation, crustal deformation, and thermal structure of the Nepal Himalaya derived from the inversion of thermochronological and thermobarometric data and modeling of the topography. *JGR* **115**, BO6407 (2010).

[20] Wobus, C., Heimsath, A., Whipple, K. & Hodges, K. Active out-of-sequence thrust faulting in the central Nepalese Himalaya. *Nature* **434**, 1008–1011 (2005).

[21] Wobus, C. W., Hodges, K. V. & Whipple, K. X. Has focused denudation sustained active thrusting at the Himalayan topographic front? *Geology* **31**, 861–864 (2003).

[22] Lavé, J. & Avouac, J. P. Active folding of fluvial terraces across the Siwaliks Hills, Himalayas of central Nepal. *JGR* **105**, 5735–5770 (2000).

[23] Lemonnier, C. *et al.* Electrical structure of the Himalaya of central Nepal: High conductivity around the mid-crustal ramp along the MHT. *GRL* **26**, 3261–3264 (1999).

[24] Nelson, K. D. *et al.* Partially Molten Middle Crust Beneath Southern Tibet: Synthesis of Project INDEPTH Results. *Science* **274**, 1684–1688 (1996).

[25] Stevens, V. & Avouac, J.-P. Coupling on the Main Himalayan Thrust. *GRL* **42**, 5828–5837 (2015).

[26] Robinson, D. M. *et al.* Kinematic model for the Main Central thrust in Nepal. *Geology* **31**, 359–362 (2003).

[27] Bollinger, L., Henry, P. & Avouac, J. P. Mountain building in the Nepal Himalaya: Thermal and kinematic model. *EPSL* **244**, 58–71 (2006).

[28] Kohn, M. J., Wieland, M. S., Parkinson, C. D. & Upreti, B. N. Miocene faulting at plate tectonic velocity in the Himalaya of central Nepal. *EPSL* **228**, 299–310 (2004).

[29] Chlieh, M., Avouac, J. P., Sieh, K., Natawidjaja, D. H. & Galetzka, J. Heterogeneous coupling of the Sumatran megathrust constrained by geodetic and paleogeodetic measurements. *JGR* **113** (2008).

[30] Loveless, J. P. & Meade, B. J. Spatial correlation of interseismic coupling and coseismic rupture extent of the 2011 M_W=9.0 Tohoku-oki earthquake. *JGR* (2011).

[31] Jolivet, R., Simons, M., Agram, P. S., Duputel, Z. & Shen, Z.-K. Aseismic slip and seismogenic coupling along the central San Andreas Fault. *GRL* **42**, 297–306 (2015).

[32] Elliott, J. R., Copley, A. C., Holley, R., Scharer, K. & Parsons, B. The 2011 Mw 7.1 Van (Eastern Turkey) earthquake. *JGR* **118**, 1619–1637 (2013).

[33] Elliott, J. R. *et al.* Depth segmentation of the seismogenic continental crust: The 2008 and 2009 Qaidam earthquakes. *GRL* **38**, L06305 (2011).

[34] Jackson, M. & Bilham, R. Constraints on Himalayan deformation inferred from vertical velocity fields in Nepal and Tibet. *JGR* **99**, 13897–13912 (1994).

[35] Grandin, R. *et al.* Long-term growth of the Himalaya inferred from interseismic InSAR measurement. *Geology* **40**, 1059–1062 (2012).

[36] Wessel, P. & Smith, W. H. F. New, improved version of generic mapping tools released. *Eos Trans. AGU* **79**, 579–579 (1998).

[37] Taylor, M. & Yin, A. Active structures of the Himalayan-Tibetan orogen and their relationships to earthquake distribution, contemporary strain field, and Cenozoic volcanism. *Geosphere* **5**, 199–214 (2009).

[38] Ekström, G., Nettles, M. & Dziewoński, A. M. The global CMT project 2004-2010: Centroid-moment tensors for 13,017 earthquakes. *PEPI* **200**, 1–9 (2012).

Acknowledgements This work was supported by the UK Natural Environmental Research Council (NERC) through the Looking Inside the Continents (LiCS) project (NE/K011006/1), the Earthquake without Frontiers (EwF) project (EwF_NE/J02001X/1_1), and the Centre for the Observation and Modelling of Earthquakes, Volcanoes and Tectonics (COMET, http://comet.nerc.ac.uk). The Sentinel-1A interferograms presented are a derived work of Copernicus data, subject to the ESA use and distribution conditions. RJ is supported by the Marie Curie FP7 Initial Training Network iTECC (investigating Tectonic Erosion Climate Couplings). We are grateful to Eric Lindsey & colleagues for making ALOS-2 displacements available at http://topex.ucsd.edu/nepal/. We thank Alex Copley, Philip England, Andy Hooper, James Jackson, Barry Parsons, Richard Walters and Tim Wright for discussions. Most figures were made using the public domain Generic Mapping Tools[36].

Author Contributions The first two authors each contributed equally to the study. J.R.E. wrote the manuscript and processed Sentinel offset data. R.J. performed the fault modelling. P.J.G. processed the Sentinel interferograms. J.P.A. conceived the research idea. J.H processed the optical offset data. M.P.S. constructed the geological cross section. V.L.S. produced the interseismic coupling map. All authors took part in finalizing the manuscript.

Additional Information Supplementary information is available in the online version of the paper. Reprints and permissions information is available online at www.nature.com/reprints. Correspondence and requests for materials should be addressed to J.R.E (john.elliott@earth.ox.ac.uk).

Competing financial interests The authors declare no competing financial interests.

[1]COMET, Department of Earth Sciences, University of Oxford, Oxford, OX1 3AN, UK, [2]COMET, Bullard Laboratories, Department of Earth Sciences, University of Cambridge, Cambridge, CB3 OEZ, UK, [3]COMET, School of Earth & Environment, University of Leeds, Leeds, LS2 9JT, UK, [4]Geological and Planetary sciences, California Institute of Technology, Pasadena, California, USA. [5]ARUP 13 Fitzroy Street, London, W1T 4BQ, UK, [6]Department of Earth Sciences, University of Oxford, Oxford, OX1 3AN, UK. *e-mail: john.elliott@earth.ox.ac.uk.

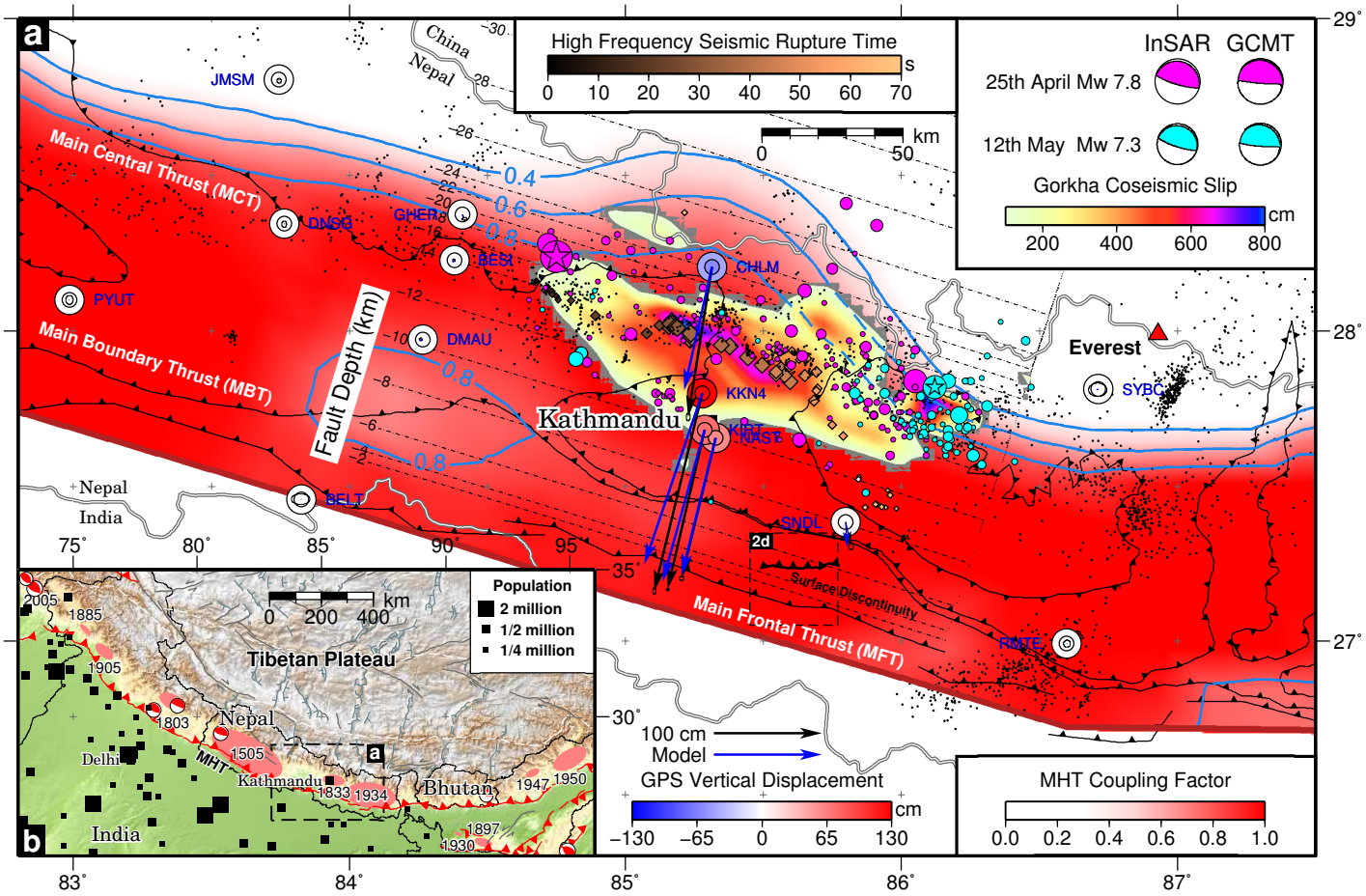

Figure 1 | Comparison of earthquake slip determined from surface geodetic displacements with long-term interseismic coupling. a. Coseismic slip distribution on the MHT (dashed depth contours) from the mainshock and largest aftershock (stars denote epicentres, circles aftershocks) and MHT coupling from interseismic deformation[25] (blue lines), and pre-earthquake background seismicity[12] (black dots). The spatio-temporal evolution of the high-frequency seismic sources during the earthquake rupture[1] follow the ramp-and-flat hinge line in our model at 14 km depth (copper diamonds). Black triangles indicate active Main Frontal Thrust trace[37] and Main Boundary and Central Thrusts. Blue-to-Red coloured circles indicate measured (inner circle) and predicted (outer circle) vertical GPS coseismic displacements, and arrows horizontal (black data, blue model). **b.** Estimated extent of ruptures due to past large earthquakes[7;10]. Magnitude 6+ reverse faulting earthquakes (1976–2015) are from the GCMT catalogue[38].

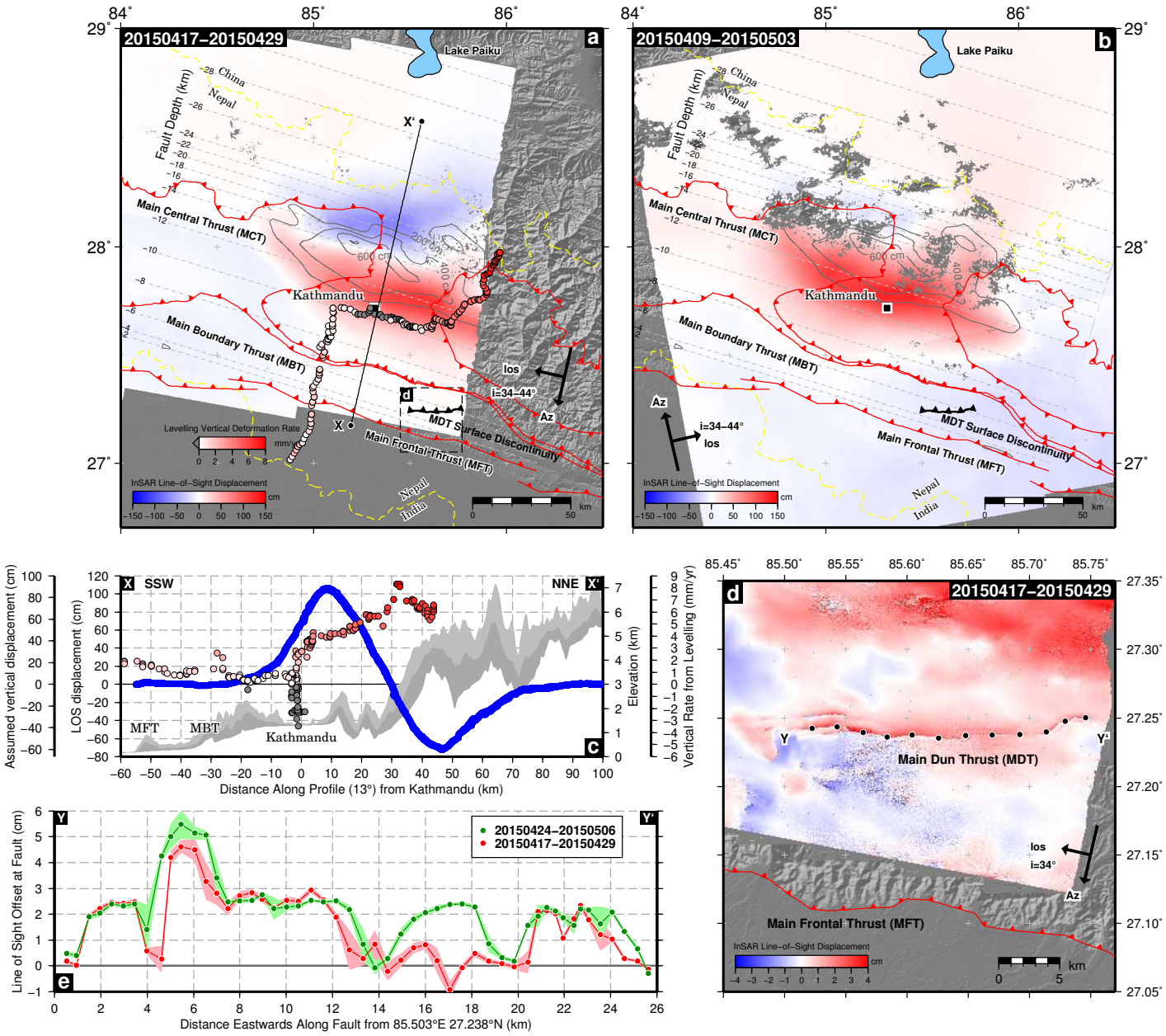

Figure 2 | Deformation patterns observed in Sentinel-1 interferograms for the 2015 Gorkha mainshock and comparison to long-term levelling data. **a.** Coseismic displacement field (positive towards satellite) with contour lines of modelled slip at depth, pre-earthquake interseismic vertical leveling rates[34] (coloured dots) and MFT surface trace[37]. **b.** Coseismic ascending interferogram. **c.** North-South profile of the deformation (blue) in (a) compared to levelling uplift rates[34] (coloured circles - negative values denote localised non-tectonic subsidence around Kathmandu). **d.** Discontinuity in the displacement field in (a) along the Main Dun Thrust (MDT), consistent with ∼12 cm of thrust motion on the MDT. Locations (black dots) of offsets given for every 4th point show in e). **e.** Displacement offsets across the MDT are consistent from independent interferograms (a,b) suggesting slip happened during, or shortly after the Gorkha earthquake, with potential increase along the central section (14–19 km).

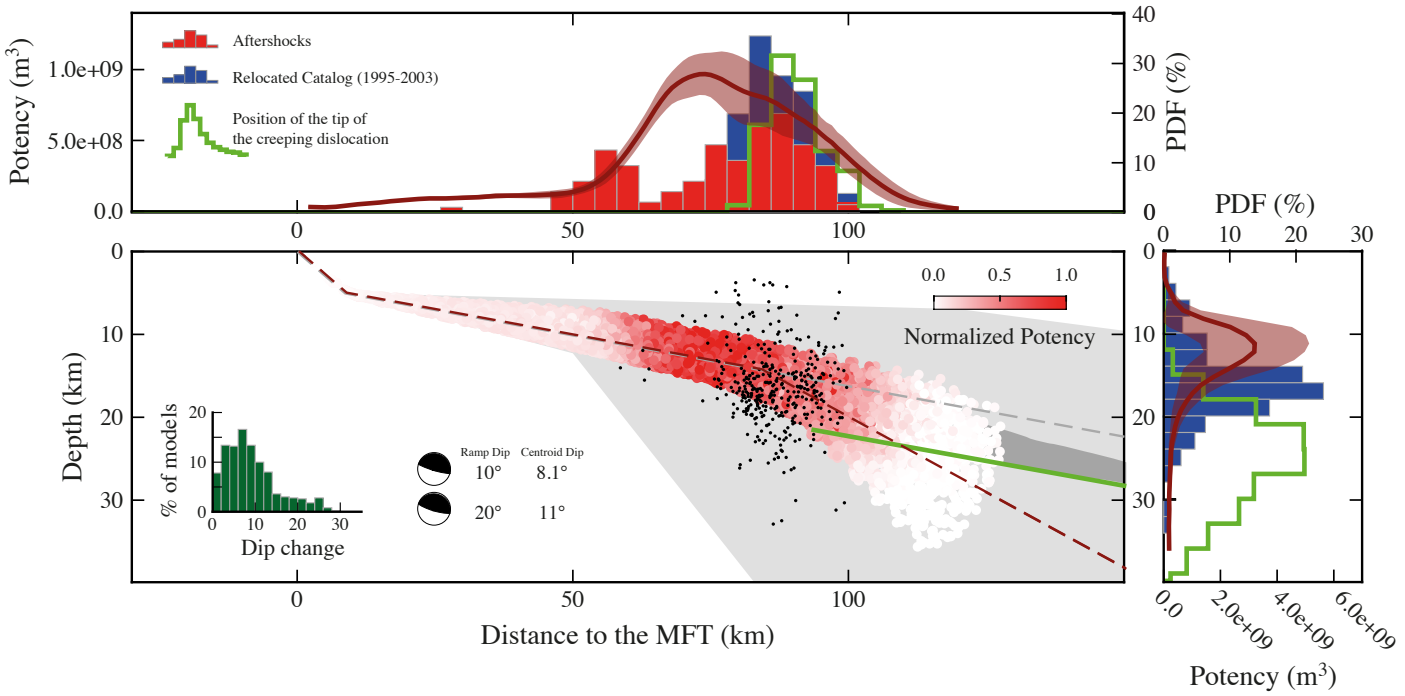

Figure 3 | MHT Geometry exploration along a cross-section (N18°). White-to-red dots are slip potency from 500 models randomly picked inside the 95% best geometries out of the total range explored (grey). Dashed brown line is our proposed geometry. Grey dashed line is an alternative model without a kink. Green line is the creeping section of the MHT re-estimated in this study. Dark grey shading indicates the location of the main reflector in the InDepth[15] Profile. Dark dots are micro-earthquakes before the Gorkha earthquake. Focal mechanisms are for two models with a 10° and 20° dip angle ramp. Dark green histogram shows the change in dip angle between flat and mid-crustal ramp for 500 acceptable models. Green histogram lines show the horizontal (top) and depth (right) location of the tip of the creeping section. Histograms show seismic activity before (1993–1995; blue) and after (red) the Gorkha earthquake. Red line and shading show mean slip potency and standard deviation for 500 acceptable models.

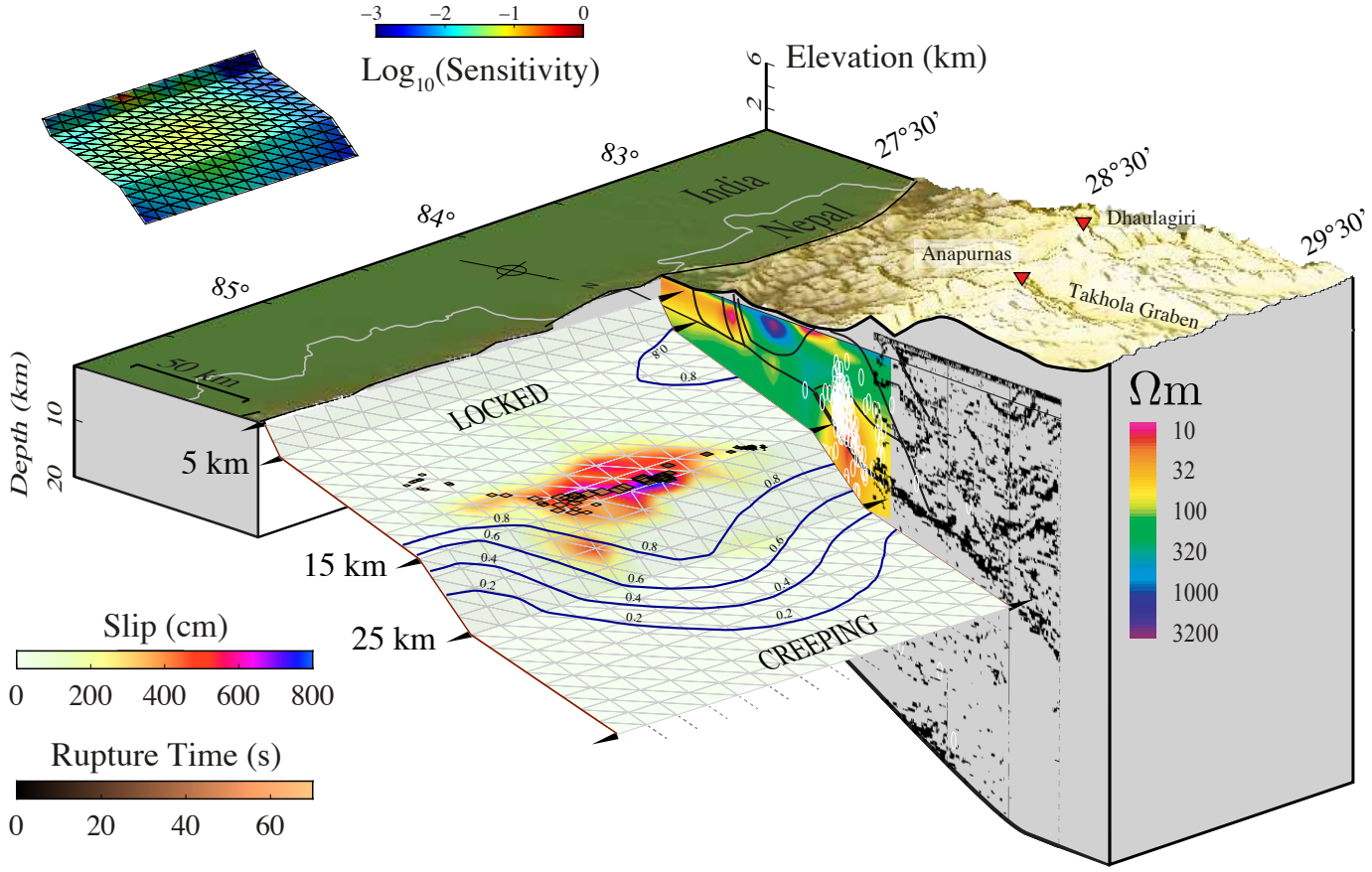

Figure 4 | Three-dimensional block diagram of the geometry proposed for the MHT. Colors denote earthquake slip relative to interseismic coupling (blue lines) inferred from GPS-, leveling- and InSAR-derived deformation rates prior to the Gorkha earthquake[25]. High-frequency seismic sources[1] during the earthquake rupture (diamonds), run along the ramp-and-flat hinge line at 14–15 km depth. The cross-section shows the InDepth reflection profile[15], the main faults (black lines) and an electromagneto-telluric image[23] highlighting the high-conductivity measured along the MHT. White ellipses are relocated micro-seismic activity prior to the Gorkha earthquake. Note the gap between the fault plane and cross section for clarity. Inset: Model sensitivity S (defined as $diag(\mathbf{G}'\mathbf{G})$ where $\mathbf{G}$ is the Green's function matrix) indicates the normalized sum of surface displacements caused by unit slip on each point on the fault.

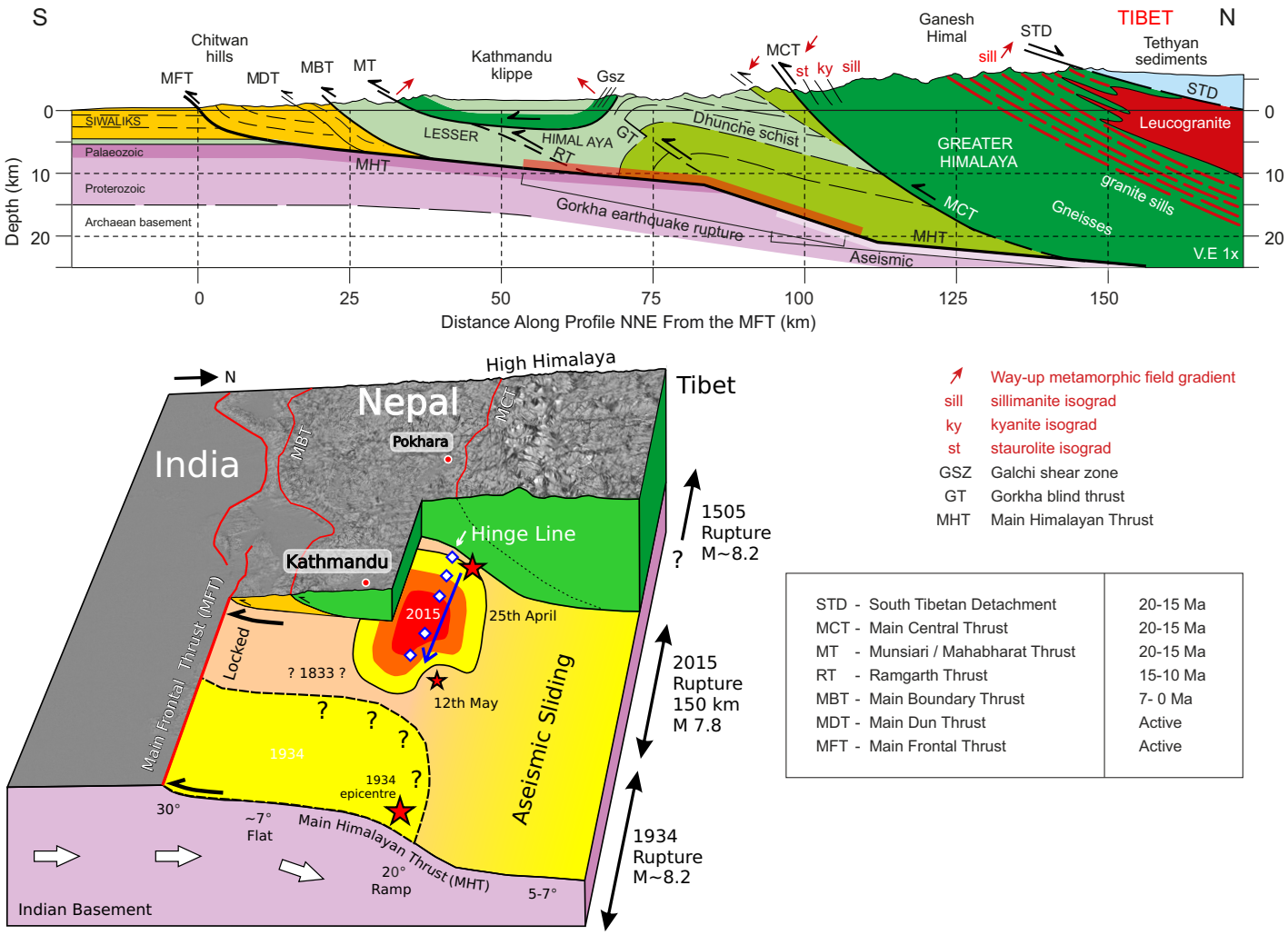

Figure 5 | Geological cross section incorporating the Main Himalayan Thrust geometry, and schematic cartoon of the 2015 rupture area relative to previous earthquakes. (top) Geological north-south profile across the Ganesh-Langtang Himalaya with periods of activity of the major Himalaya Thrusts denoted. (bottom) Location of the 2015 earthquake and its aftershock on the resolved MHT geometry (with the upper plate removed to reveal the slip zone). High-frequency seismic sources[1] are marked as diamonds running along the hinge line between the ramp and flat. The Mw 7.2 aftershock occurred at the eastern end of the main rupture. The rupture extents of previous earthquakes from 1934 (M~8.2), 1833 (M~7.6) and 1505 (M~8.2) are poorly constrained.

Figure 1

Figure 2

Figure 3

Figure 4

Figure 5

Figure 6

Figure 7

Figure 8

Figure 9

Figure 10

Figure 11

Figure 12

Table 1